EFFECT OF ORGANOCLAY MODIFICATION ON THE MECHANICAL, MORPHOLOGY, AND THERMAL PROPERTIES OF INJECTION MOLDED POLYAMIDE 6/POLYPROPYLENE/MONTMORILLONITE NANOCOMPOSITES

Z.A. Mohd Ishak [1*], Kusmono [1], W.S. Chow [1], T. Takeichi [2], Rochmadi [3]

[1]School of Materials and Mineral Resources Engineering, Universiti Sains Malaysia, Penang-Malaysia – zarifin.ishak@googlemail.com
[2]Toyohashi University of Technology, Toyohashi-Japan – takeichi@tutms.tut.ac.jp
[3]Department of Chemical Engineering, Gadjah Mada University, Yogyakarta-Indonesia – rochmadister@gmail.com

Polyamide 6/polypropylene (PA6/PP = 70/30 parts) blends containing 4 phr (parts per hundred resin) of organophilic montmorillonite (OMMT) were prepared by melt compounding using co-rotating twin-screw extruder followed by injection molding. The effect of organoclay modification on the mechanical and morphological properties of nanocomposites were investigated by using x-ray diffraction (XRD), transmission electron microscopy (TEM), tensile, flexural, and impact tests. The thermal stability and thermal properties of nanocomposites was characterized by using thermogravimetric analysis (TGA) and differential scanning calorimetry (DSC). The morphology and properties of the PA6/PP nanocomposites were determined by the alkyl ammonium salt length, that is, the hydrophobicity of the organic modifier. XRD and TEM revealed the formation of exfoliated structure for the nanocomposites prepared using stearylamine modified montmorillonite and commercial organoclay. On the contrary, a mixture of intercalated and exfoliated structures was observed for the nanocomposites prepared using 12-aminolauric acid and dodecylamine modified montmorillonite. Incorporation of OMMT into PA6/PP matrix increased stiffness and strength but at the expense of ductility. The nanocomposite prepared using stearylamine modified montmorillonite displayed the best mechanical properties and thermal stability. This was attributed to better exfoliated structure in the nanocomposites.

Introduction

Polymer/clay nanocomposites (PCNs) have received special attention because of their improved properties at very low clay loading levels compared with conventional filler composites. Among these improved properties are mechanical, dimensional, barrier to the different gases, thermal stability, and flame retardant enhancements with respect to the bulk polymers [1]. Clay minerals such as montmorillonite (MMT) exhibit many interesting structural features including exchangeable interlayer cations, hydroxyl groups on the edges of clay platelets, and a high aspect ratio of the individual layers. However, the pristine silicate surface is generally too hydrophilic to be compatible with most polymers. To render the hydrophobic clay surface, they are intercalated with organic cations such as alkylammonium salt by a cation exchange reaction [2].

Blends of PA6 and PP have received much attention because they combine the thermomechanical properties of PA6 with the insensitivity to humid environments and easy processing characteristics of PP. Nanocomposites based on PA6/PP blends using commercial organoclay have been studied extensively by many researchers [3-4]. Recently, several studies on the effect of organic modifier for clay modification on the morphology and mechanical properties of PCNs have been carried out. Reichert et al [5] investigated the effects of the length of the alkyl group on the amine used to modify sodium fluoromica on the morphology and mechanical properties of PP nanocomposites obtained by melt compounding. A critical alkyl length of 12 carbons or more was found necessary for promoting exfoliation. Usuki et al. [6] showed that swelling of MMT modified with ω-amino acids by ε-caprolactam increased significantly when the carbon number of the amino acid was greater than 8. To our knowledge, preparation and characterization of PA6/PP nanocomposites using clay modification was still limited.

In this study, PA6/PP/OMMT nanocomposites were prepared by melt compounding technique. Sodium montmorillonite (Na-MMT) was modified with dodecylamine, 12-aminolauric acid, and stearylamine to evaluate the effect of clay modification on the morphology, mechanical, and thermal properties of PA6/PP nanocomposites. The intercalation/exfoliation of the clays within polymer matrix was evaluated using x-ray diffraction (XRD) and transmission electron microscopy (TEM). The mechanical properties were determined through tensile, flexural, and izod impact tests. The thermal stability and thermal properties were characterized using thermogravimetric analysis (TGA) and differential scanning calorimetry (DSC).

Experimental

Materials

PA6 (Amilan CM 1017) used in this study was a commercial product of Toray Nilon Resin AMILAN, Japan. PP (Pro-Fax SM-240) was purchased from Titan Himont Polymer (M) Sdn. Bhd., Malaysia. Kunipia-F, sodium montmorillonite (Na-MMT) clay with cation exchange capacity (CEC) of 119 mEq/100 g, was supplied by Kunimine Industry Co., Japan. Three different types of alkyl ammonium salts used to modify Na-MMT were dodecylamine [NH_2 CH_3 $(CH_2)_{11}$], 12 aminolauric acid [NH_2 $(CH_2)_{11}COOH$], and stearylamine [NH_2 CH_3 $(CH_2)_{16}$ CH_2], respectively. A commercial organoclay (Nanomer I.30TC) supplied by Nanocor, Inc., USA containing montmorillonite (70 wt %) intercalated by octadecylamine (30 wt %) was also used.

Preparation of OMMT

Organophilic montmorillonite (OMMT) was prepared by cation exchange of MMT with various alkyl ammonium salts according to a method reported by Agag and Takeichi [7]. Modification of MMT by dodecyl ammonium chloride was carried as follows. Dodecyl ammonium chloride solution was prepared by the addition of 4.17 g of conc. HCl (40 mmol) to 7.41 g of dodecylamine (40 mmol) in 1000 ml of distilled water. The mixture was stirred at 80 ºC until a clear solution was obtained. To this solution, a suspension of 20 g of MMT in 1000 ml of distilled water was added and then stirred at 80 ºC for 5 hours. The obtained white precipitate was collected by suction filtration and then poured into hot water (ca. 60 ºC) followed by stirring for 2 hours to remove salt. This process was repeated several times until no chloride was detected in the filtrate by 0.1 N $AgNO_3$. The resultant was air-dried, ground in mortar, sieved, and finally dried in an air-blowing oven at 110 ºC for 3 days. The dodecylamine modified MMT was termed D-MMT. The modification of MMT with 12-aminolauric acid or stearylamine followed the aforementioned procedure, except that 8.61 g of 12-aminolauric acid (40 mmol) or 10.78 g of stearylamine (40 mmol) was used instead of 7.41 g of dodecylamine (40 mmol). Further, the MMT modified with 12-aminolauric acid and stearylamine were denoted A-MMT and S-MMT, respectively. The commercial organoclay was denoted C-MMT.

Preparation of PA6/PP/OMMT nanocomposites

PA6/PP (70/30) and OMMT (4 phr) were melt-mixed in a co-rotating intermeshing twin-screw extruder (BERSTORFF ZE 25) at temperature ranging from 230 to 240°C and a screw speed of 70 rpm. The extrudates were pelletized with a pelletizer and then injection-molded into standard tensile bars (ASTM D638 type I) and flexural specimens (ASTM D790) using an injection molding machine (Haitian HTF160X). The barrel zone temperatures were set at 190, 235, 250, 255, 260, and 250 ºC and a mold temperature of 110°C. Prior to melt-mixing and injection molding, all pellets were dried in an oven at 80 ºC for 15 hours.

Fourier Transform Infra-Red Spectroscopy (FT-IR)

Fourier transform infra-red spectroscopy (FT-IR) analyses of Na-MMT and OMMT were carried out with JASCO spectrophotometer model FT/IR-420 at wave number from 400-4000 cm^{-1}.

X-Ray Diffraction (XRD)

The diffraction studies were performed in reflection mode using X-ray diffractometer, Rigaku RINT2000 using CuK_α radiation at a scan rate of 0.3°/min in a 2θ range of 2-10°, and operated at 30 kV and 20 mA.

Transmission Electron Microscopy (TEM)

TEM measurements were carried out with a JEOL JEM-200CX TEM operating at an accelerating voltage of 200 kV. The specimens were prepared using a Leica Ultracut UCT ultramicrotome. Ultra-thin sections of about 60 nm in thickness were cut with a diatome diamond knife (35°) at room temperature.

Mechanical Properties

Tensile and flexural tests were carried out with a universal testing machine (Instron 3366) at room temperature according to ASTM D638 type I and ASTM D790, respectively. Tensile test was performed at a crosshead speed of 50 mm/min. For flexural test, a three-point bending configuration was selected with a support span length of 50 mm and a crosshead speed of 3 mm/min. Izod impact test was carried out on notched specimens using a Pendulum Hammer Impact 25 S/N V67R (Galdabini) according to ASTM 256-02 with a impact speed of 3.46 m/s.

Thermogravimetric Analysis (TGA)

The thermal stability of organoclay, PA6/PP blend, and its nanocomposites was studied using thermogravimetric analysis (TGA; Perkin-Elmer TGA-6). The sample was heated from room temperature to 600°C at 10°C/min under nitrogen atmosphere.

Differential Scanning Calorimetry (DSC)

The melting and crystallization behaviors of PA6/PP blend and its nanocomposites were characterized using differential scanning calorimetry (DSC) using Rigaku Thermo Plus 2 DSC8230 in nitrogen atmosphere.

Results and Discussion

Figure 1 shows the FTIR spectra of Na-MMT and OMMT. The characteristic absorption bands of Na-MMT and OMMT are shown by peaks at 3629 cm^{-1} (O-H stretching), 1643 cm^{-1} (H-O bending), 1043 cm^{-1} (Si-O stretching), 914 cm^{-1} (O-H bending), and 521 cm^{-1} (Si-O bending). In addition to those peaks, the OMMT also exhibit peaks at 3251 cm^{-1} (N-H stretching), 2920 cm^{-1} (-CH_3 stretching), 2850 cm^{-1} (-CH_2 stretching), and 1469 cm^{-1} (-CH_2 stretching). For

A-MMT, there is a new peak at 1713 cm^{-1} corresponding to –COOH. These results indicate that the alkylammonium chains have been intercalated into the galleries of MMT by a cation exchange reaction.

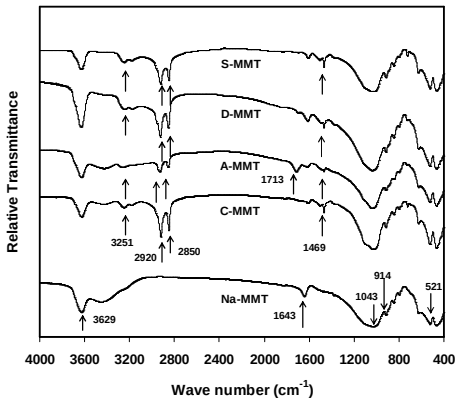

Figure 1. FTIR spectra of Na-MMT and OMMT

Figure 2 shows the XRD patterns of Na-MMT and OMMT. The Na-MMT, D-MMT, A-MMT, S-MMT, and C-MMT patterns reveal the characteristic diffraction peaks at 7.12°, 5.44°, 5.02°, 3.98°, and 3.48° respectively, corresponding to basal spacing (d_{001}) of 1.24 nm, 1.62 nm, 1.76 nm, 2.22 nm, and 2.54 nm, respectively. Thus, OMMT exhibited a larger basal spacing than Na-MMT. This could be associated with the intercalation of the alkyl ammonium chains into galleries of MMT, in agreement with the above FTIR results. The basal spacing was increased in the order of Na-MMT < D-MMT < A-MMT < S-MMT < C-MMT. The basal spacing of S-MMT and C-MMT were greater than that of both D-MMT and A-MMT because the alkyl chains length of S-MMT and C-MMT were longer than that of both D-MMT and A-MMT. The basal spacing of A-MMT was greater than that of D-MMT due to larger dimension of the –COOH group in A-MMT than $–CH_3$ in the D-MMT. Morover, there are the two functional groups in the A-MMT, namely amine and carboxylic acid groups.

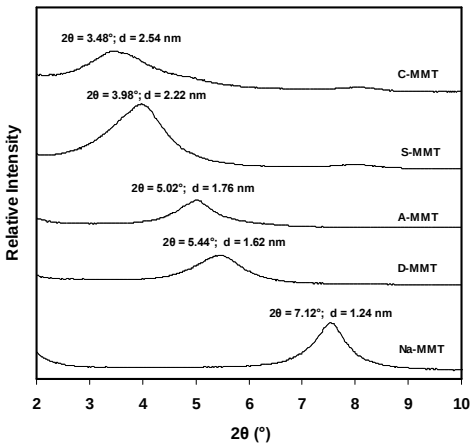

Figure 2. XRD patterns of Na-MMT and OMMT

Figure 3 shows the XRD patterns of PA6/PP blend and its nanocomposites. The PA6/PP/4Na-MMT composite exhibits a diffraction peak at about 2θ = 6.29°, corresponding to a basal spacing of 1.40 nm. Accordingly, there was a slight increase in basal spacing from 1.24 nm for Na-MMT to 1.4 nm for PA6/PP/4Na-MMT composite. This indicates that the polymer molecular chains have entered the gallery of MMT and the intercalated structure was formed. A broad shoulder peak appears at about 2θ = 2.99° and 3.89°, corresponding to basal spacing of 2.95 and 2.05 nm for PA6/PP/4D-MMT and PA6/PP/4A-MMT composites, respectively. The presence of a broad shoulder peak probably indicates the formation of partially exfoliated/partially intercalated structures. For both PA6/PP/4S-MMT and PA6/PP/4C-MMT nanocomposites, the absence of diffraction peak indicates the delamination and dispersion of the clay nanolayers within polymer matrix, i.e. the formation of an exfoliated structure in both nanocomposites.

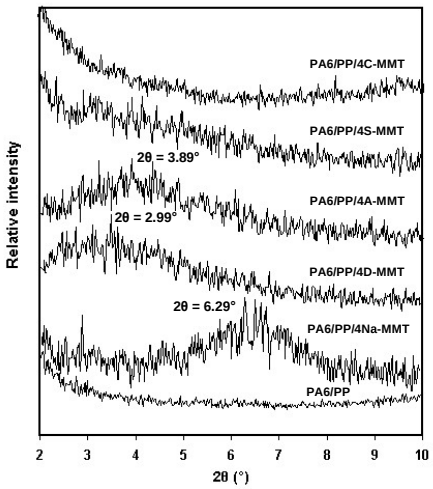

Figure 3. XRD patterns of the PA6/PP blend and its nanocomposites

Figure 4 shows the TEM images of PA6/PP/4Na-MMT, PA6/PP/4D-MMT, PA6/PP/4S-MMT, and PA6/PP/4C-MMT nanocomposites. The PA6/PP/4Na-MMT (Fig. 4a) exhibits poor dispersion of clay platelets, where intercalated clay layers stacks and clay aggregates can be observed. This may be attributed to the presence of strong electrostatic forces between clay layers [8]. In case of PA6/PP/4D-MMT (Fig. 4b), most of the clay layers are exfoliated as monolayer, but intercalated clay layers stacks are still observed. No any discernible clay platelets can be seen in the PP phase. For both PA6/PP/4S-MMT and PA6/PP/4C-MMT (Fig. 4c and 4d), the individual clay platelets are dispersed homogenously in the PA6 phase, suggesting an exfoliated structure was formed in both nanocomposites. Compared with the PA6/PP/4D-MMT, both PA6/PP/4S-MMT and PA6/PP/4C-MMT exhibited better dispersion and exfoliation of silicate layers in PA6 phase. This may be attributed to the larger alkyl length on the organic modifier for

stearylamine and octadecylamine modified MMT than dodecylamine modified MMT. Increase in the alkyl length of organoclay resulted in an increase in basal spacing as discussed earlier by XRD results. As a result, diffusion of polymer chains into MMT galleries is easier due to increased spacing and ultimately leads to improved exfoliation [9]. Thus, the structure of organic modifier (alkyl ammonium chain length) within organoclay is an important factor to affect the morphology of PA6/PP/organoclay nanocomposites.

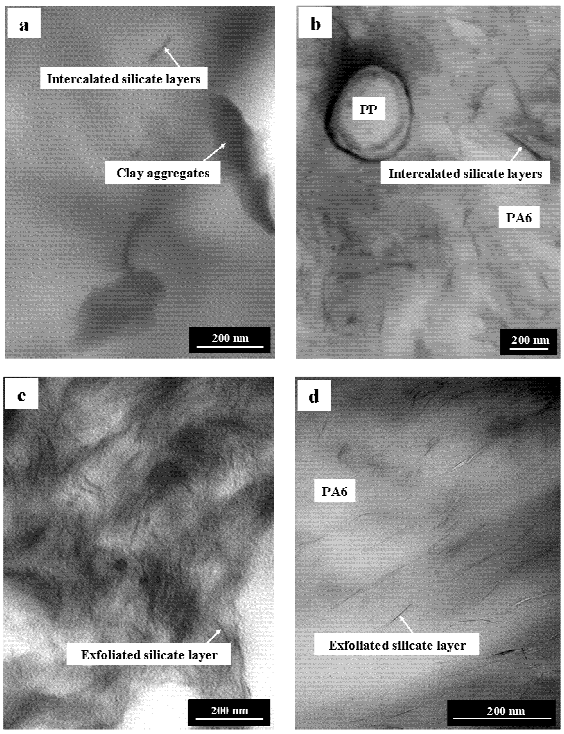

Figure 4. TEM images of :
a. PA6/PP/4Na-MMT; b. PA6/PP/4D-MMT;
c. PA6/PP/4S-MMT; d. PA6/PP/4C-MMT

Mechanical Properties
Tensile Properties

Table 1 shows the tensile properties of PA6/PP blend and its nanocomposites. It can be seen that the addition of both Na-MMT and OMMT into PA6/PP matrix significantly increased its tensile modulus. This was attributed to the reinforcement effect of the rigid inorganic clay and the constraining effect of silicate layers on molecular motion of polymer molecular chains [10]. The PA6/PP/4S-MMT nanocomposite showed the highest tensile modulus and strength followed by the ones containing C-MMT, A-MMT, and then D-MMT. The better reinforcement effect of S-MMT could be associated with the larger initial basal spacing of S-MMT than D-MMT and A-MMT. The larger initial basal spacing comes from larger alkyl chain length of carbon atoms in organic modifier of organocaly. With larger basal spacing, the diffusion of polymer chains into MMT galleries is easier and then leads to improved exfoliation. When the clay particles are dispersed more finely (exfoliated), we can get a higher aspect ratio of the dispersed particles and a larger interfacial area, both of which make stress transfer to the silicate layers much more effective; this will lead to improvements of the tensile properties [11]. Thus, the length of alkyl group of organic modifier in the organoclay affected the mechanical properties of PA6/PP nanocomposites.

It is also noted from Table 1 that the incorporation of both Na-MMT and OMMT into the PA6/PP matrix decreased its elongation at break due to constraint effect of clay on mobility of polymer chains. The elongation at break of PA6/PP/4Na-MMT was higher than that of PA6/PP/OMMT nanocomposites. This may be attributed to the intercalated structure in the PA6/PP/4Na-MMT composite. Masenelli-Varlot et al. [12] reported that the intercalated PA6/clay nanocomposites had a higher elongation at break than exfoliated nanocomposites.

Table 1. Tensile properties of PA6/PP blend and its nanocomposites

Sample designation	Tensile modulus (GPa)	Tensile strength (MPa)	Elongation at break (%)
PA6/PP	1.8 ± 0.0	39.9 ± 0.8	11.9 ± 1.1
PA6/PP/4Na-MMT	2.0 ± 0.0	38.2 ± 1.7	8.0 ± 1.1
PA6/PP/4D-MMT	2.0 ± 0.0	38.7 ± 0.5	2.7 ± 0.1
PA6/PP/4A-MMT	2.1 ± 0.0	39.4 ± 1.0	2.8 ± 0.2
PA6/PP/4S-MMT	2.2 ± 0.0	43.8 ± 1.4	2.9 ± 0.1
PA6/PP/4C-MMT	2.0 ± 0.0	43.2 ± 0.5	3.5 ± 0.1

Flexural Properties

Table 2 demonstrates the flexural and impact properties of the PA6/PP blend and its nanocomposites. The incorporation of both Na-MMT and OMMT remarkably increased the flexural modulus and slightly increased the flexural strength of PA6/PP blend. These improvements could be attributed to high stiffness and aspect ratio of silicate layers [13]. Compared with the PA6/PP/4Na-MMT composite, the flexural modulus and strength of PA6/PP/4OMMT nanocomposites were higher because of the nanoscale structure, the large aspect ratio, the large surface area of the layered silicates, and the corresponding strong interaction between polymer molecules chains and silicate surface [14]. The highest flexural properties observed in the PA6/PP/4S-MMT could again be attributed to better exfoliated structure in this nanocomposite.

Table 2. Flexural and impact properties of PA6/PP blend and its nanocomposites

Sample designation	Flexural modulus (GPa)	Flexural strength (MPa)	Impact strength (kJ/m^2)
PA6/PP	1.9 ± 0.1	62.5 ± 1.3	5.47 ± 0.45
PA6/PP/4Na-MMT	2.3 ± 0.1	66.8 ± 1.3	3.58 ± 0.18
PA6/PP/4D-MMT	2.6 ± 0.0	61.1 ± 1.0	1.55 ± 0.05
PA6/PP/4A-MMT	2.4 ± 0.0	63.2 ± 1.2	1.65 ± 0.11
PA6/PP/4S-MMT	2.7 ± 0.0	69.5 ± 1.2	1.76 ± 0.04
PA6/PP/4C-MMT	2.3 ± 0.0	63.8 ± 0.9	1.74 ± 0.05

Impact Strength

Table 2 also shows the impact strength of PA6/PP blend and its nanocomposites. The addition of both Na-MMT and OMMT into PA6/PP matrix drastically decreased its impact strength. The reduction in the impact strength could be attributed to the immobilization of the macromolecular chains by the clay particles, which limited their ability to adapt to the deformation and make the material more brittle. In addition, each silicate layer or aggregates of silicate layers was the site of stress concentration and could act as a micro crack initiator [15]. According to Nair [16], the reduction in toughness of polyamide 6,6/clay nanocomposites may be caused by the formation of micro voids or micro cracks in the crack-tip region and tend to reduce toughness.

Thermogravimetric Analysis (TGA)

The TGA curves of Na-MMT and OMMT are shown in Figure 5. Below 100°C, Na-MMT exhibits a relatively higher weight loss than OMMT, corresponding to the removal of water from interlayers coordinated to Na^+. For OMMT, the weight loss in this temperature is low because of the organophilic properties of OMMT containing alkyl ammonium ions [17]. In the temperature range of 100-600°C for Na-MMT, the weight loss may be attributed to the decomposition of hydrogen-bonded water molecules and some of the OH group from tetrahedral sheets [18]. On the other hand, the OMMT shows greater weight losses than Na-MMT in this temperature range. The weight losses for OMMT could be explained mainly by the decomposition of intercalated ammonium and partly by the adsorbed water molecules below 220°C [19]. In the temperature range of 600-850°C, the weight losses for Na-MMT and OMMT was probably associated with the dehydroxylation of Na-MMT [20]. It can also be noted from Figure 5 that Na^+ has been well ion exchanged with the alkyl amines as shown by the reduction of weight in OMMT. The shorter chain length of alkyl amine exhibited the smaller reduction in weight.

Figure 6 shows the TGA curves of PA6/PP blend and its nanocomposites. The weight losses between 150 and 400°C could be attributed to the thermal decomposition of alkyl ammonium ions in the modified clay [21]. According to Liu et al. [22], the onset of decomposition temperature was characterized by the temperature at 5% weight loss ($T_{5\%}$). The onset of decomposition temperatures of PA6/PP, PA6/PP/4Na-MMT, PA6/PP/4D-MMT, PA6/PP/4A-MMT, PA6/PP/4S-MMT, and PA6/PP/4C-MMT were 358, 362, 371, 375, 365, and 354°C, respectively. This indicates that the onset of degradation temperature of PA6/PP matrix was slightly increased in the presence of both Na-MMT and OMMT. The improved thermal stability could be associated with the clay as an inorganic material with high thermal stability and great barrier properties that can prevent the heat from transmitting quickly and can limit the continuous decomposition [23]. In the temperature range of 400-500°C, the PA6/PP/4S-MMT and PA6/PP/4C-MMT nanocomposites exhibited higher decomposition temperature than others. The dispersed nanoscale silicate layers in the polymer matrix could be more effective in hindering diffusion of volatile decomposition products, leading to the improved thermal stability for both PA6/PP/4S-MMT and PA6/PP/4C-MMT nanocomposites.

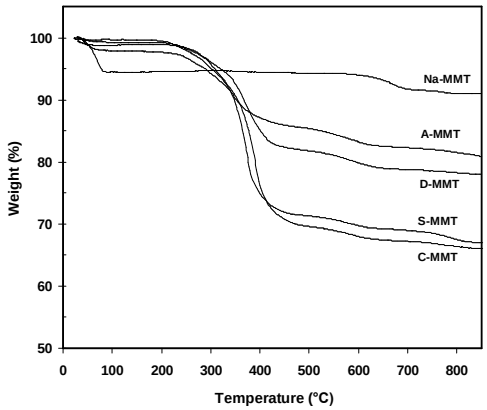

Figure 5. TGA curves of Na-MMT and OMMT

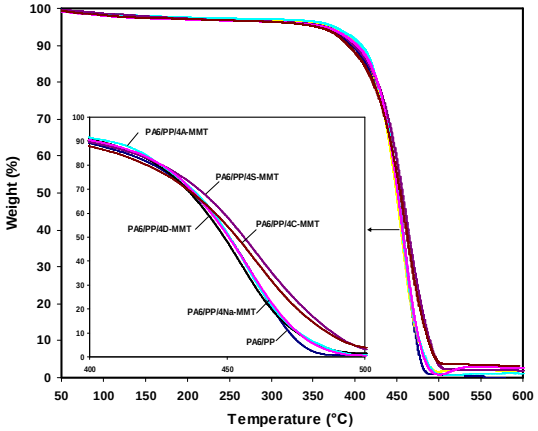

Figure 6. TGA curves of PA6/PP blend and its nanocomposites

Differential Scanning Calorimetry (DSC)

Figures 7 and 8 show the DSC heating and cooling scans of PA6/PP blend and its nanocomposites, respectively. The melting temperature (T_m), crystallization temperature (T_c), and the degree of crystallinity (X_C, %) of PP and PA6 components are summarized in Table 3. It can be seen that all samples exhibited two strong peaks, i.e. at around 161-164°C and 220-221°C which correspond to the melting temperatures of PP and the α-form crystal of PA6, respectively. With the exception of PA6/PP/4S-MMT, the addition of both Na-MMT and OMMT into PA6/PP matrix increased slightly the melting temperatures of PP and PA6. However, the addition of S-MMT into PA6/PP matrix decreased drastically the melting temperature of PA6, i.e. from 221 to 215°C, corresponding to the melting temperature of γ crystal form of PA6 phase. This suggests that the presence of S-MMT promoted the phase transformation from α to γ for PA6 phase. The may be attributed to the better dispersion and exfoliation of S-MMT in the PA6/PP matrix. The introduction of nanoclay filler into the polymer matrix had a strong heterogeneous nucleation effect, which was favorable for the formation of the less stable γ-form crystals of PA6 [24]. With the exception of PA6/PP/4Na-MMT and PA6/PP/4A-MMT, the crystallization temperature of PP was decreased in all samples. In addition, the presence of clay led to a decrease in the crystallization temperature of PA6 in the nanocomposites, regardless of both Na-MMT and OMMT. This could be attributed to the retarding effect of the silicate layers on the PP and PA6 crystals growth. With the exception of PA6/PP/4C-MMT, the incorporation of both Na-MMT and OMMT into PA6/PP matrix decreased the degree of crystallinity of both PP and PA6. This may be attributed to the physical hindrance of MMT layers to the motion of polymer molecular chains tends to retard the crystallization of polymer phase of nanocomposites reinforced with MMT clays, leading to a decrease in the degree of crystallinity [24].

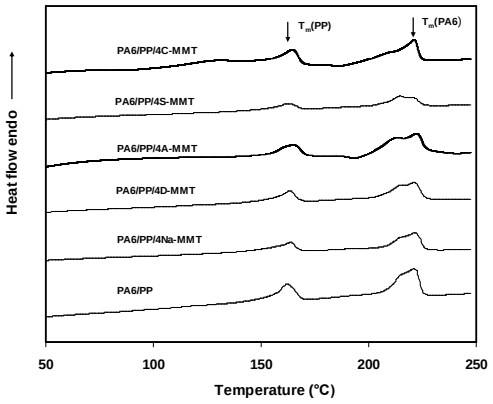

Figure 7. DSC heating scans of PA6/PP blen and its nanocomposites

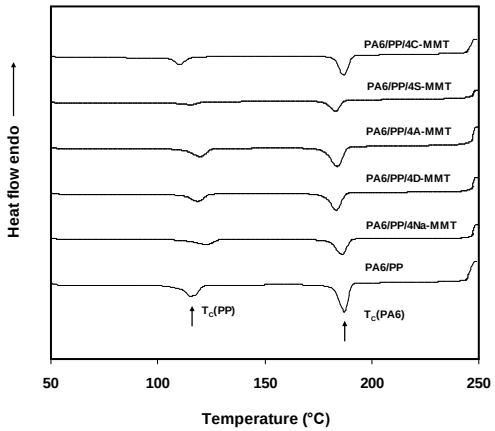

Figure 8. DSC cooling scans of PA6/PP blend and its nanocomposites

Table 3. DSC results of PA6/PP blend and its nanocomposites

Sample designation	T_m (PP) (°C)	T_c (PP) (°C)	X_C (PP) (%)	T_m (PA6) (°C)	T_c (PA6) (°C)	X_C (PA6) (%)
PA6/PP	162	119	27	221	188	26
PA6/PP/4Na-MMT	164	123	20	222	186	17
PA6/PP/4D-MMT	164	119	20	221	183	18
PA6/PP/4A-MMT	164	120	22	222	184	19
PA6/PP/4S-MMT	163	116	12	215	183	11
PA6/PP/4C-MMT	164	116	27	220	187	27

Conclusions

PA6/PP/organoclay nanocomposites were prepared by melt compounding. XRD and TEM results indicated the formation of exfoliated structure for the nanocomposites containing S-MMT and commercial organoclay, whereas a mixture of intercalated and exfoliated structures for the nanocomposites containing A-MMT and D-MMT. Incorporation of both Na-MMT and OMMT increased the stiffness but decreased the ductility and toughness of PA6/PP matrix. The tensile strength of PA6/PP matrix was decreased by addition of Na-MMT, D-MMT, and A-MMT. This may be attributed to the intercalated structures for these nanocomposites. The higher tensile strength for PA6/PP/4S-MMT and PA6/PP/4C-MMT could be attributed to better exfoliated structure in these nanocomposites. The thermal stability of PA6/PP matrix was improved with the presence of both Na-MMT and OMMT. The addition of S-MMT promoted the formation of γ crystal of PA6.

Acknowledgements

The financial support of AUN/SEED-Net JICA Project grant no: 6050071 is gratefully acknowledged. Kusmono thanks JICA for a short-term study program at Toyohashi Univeristy of Technology, Japan.

References

1. M. Alexandre M; P. Dubois P. *Materials Science and Engineering R Report* 2000, *28*, 1.
2. E.P. Giannelis; R. Krsihnamoorti; E. Manias *Adv. Polym. Sci.* 1999, *138*, 107.
3. W.S. Chow; Z.A. Mohd Ishak; J. Karger-Kocsis; A.A. Apostolov; U.S. Ishiaku *Polymer* 2003, *44*, 7427.
4. W.S. Chow; Z.A. Mohd. Ishak; U.S. Ishiaku; J. Karger-Kocsis; A.A. Apostolov *J. Appl. Polym. Sci.* 2004, *91*, 175.
5. P. Reichert; H. Nitz; S. Klinke; R. Brandsch; R. Thomann; R. Mulhaupt *Macromol. Mater. Eng.* 2000, *275*, 8.
6. A. Usuki; Y. Kojima; M. Kawasumi; A. Okada; Y. Fukushima; T. Kurauchi; O. Kamigaito *J. Mater. Res.* 1993, *8*, 1179.
7. T. Agag; T. Takeichi *Polymer*. 2000, *41*, 7083-7090.
8. Z.Z. Yu; C. Yan; M. Yang; Y.W. Mai *Polym. Int.* 2004, *53*, 1093.
9. T.D. Fornes; P.J. Yoon; D.L. Hunter; H. Keskkula; D.R. Paul *Polymer*. 2002, *43*, 5915.
10. T. Liu; W.C. Tjiu; C. He; S.S. Na; T.S. Chung *Polym. Int*. 2004, *53*, 392.
11. J.W. Lee; M.H. Kim; W.M. Choi; O.O. Park *J. Appl. Polym. Sci.* 2006, *99*, 1752.
12. K. Masenelli-Varlot; E. Reynaud; G. Vigier; J. Varlet *J. Polym. Sci. Part B: Polym. Phys.* 2002, *40*, 272.
13. S. Parija; S.K. Nayak; S.K. Verma; S.S. Tripathy *Polym. Compos.* 2004, *25*, 646.
14. W. Shishan; J. Dingjun; O. Xiaodong; W. Fen; S. Jian *Polym. Eng. Sci.* 2004, *44*, 2070.
15. P. Mareri; S. Bastide; N. Binda; A. Crespy *Compos. Sci. Tech.* 1998, *58*, 747.
16. S.V. Nair; L.O.Goettler; B.A. Lysek *Polym. Eng. Sci.* 2002, *42*, 1872.
17. H. Zheng; Y. Zhang; Z. Peng; Y. Zhang *J. Appl. Polym. Sci.* 2004, *92*, 638.
18. H.J. Bray; S.A.T. Redfern; S.M. Clark *Mineralogical Magazine*. 1998, *62*, 647.
19. P. Bala; B.K. Samantaray; S.K. Srivastava *Materials Research Bulletin*. 2000, *35*, 1717.
20. H.V. Olphen; J.J. Fripiat JJ. *Data handbook for clay materials and other non-metallic Minerals*; Pergamon: Oxford, 1979.
21. D. Yebassa; S. Balakrishnan; E. Feresenbet; D. Raghavan; P.R. Start; S.D. Hudson *J. Polym. Sci. Part A: Polym. Chemis.* 2004, *42*, 1310.
22. T. Liu; K.P. Lim; W.C. Tjiu; K.P. Pramoda; Z.K. Chen *Polymer*. 2003, *44*, 3529.
23. W. Zhang; Y. Liang; W. Luo; Y. Fang *J. Polym. Sci. Part A: Polym.Chemis.* 2003, *41*, 321.
24. C.C.M. Ma; C.T. Kuo; H.C. Kuan; C.L. Chiang *J. Appl. Polym Sci.* 2003, *88*, 1686.